HHS Public Access

Author manuscript

ACS Chem Biol. Author manuscript; available in PMC 2018 February 19.

Published in final edited form as:

ACS Chem Biol. 2012 September 21; 7(9): 1576–1585. doi:10.1021/cb3002057.

Temporal and fluoride control of secondary metabolism regulates cellular organofluorine biosynthesis

Mark C. Walker[§], **Miao Wen**[‡], **Amy M. Weeks**[‡], and **Michelle C. Y. Chang**[*,‡,§]

[‡]Department of Chemistry, University of California, Berkeley, Berkeley, CA 94720-1460

[§]Department of Molecular and Cell Biology, University of California, Berkeley, Berkeley, CA 94720-1460

Abstract

Elucidating mechanisms of natural organofluorine biosynthesis is essential for a basic understanding of fluorine biochemistry in living systems as well as for expanding biological methods for fluorine incorporation into probe or therapeutic molecules. To meet this goal we have combined massively parallel sequencing technologies, genetic knockout, and *in vitro* biochemical approaches to investigate the fluoride response of the only known genetic host of an organofluorine producing pathway, *Streptomyces cattleya*. Interestingly, we have discovered that the major mode of *S. cattleya*'s resistance to the fluorinated toxin it produces, fluoroacetate, may be due to temporal control of production rather than the ability of the host's metabolic machinery to discriminate between fluorinated and non–fluorinated molecules. Indeed, neither the acetate kinase/phosphotransacetylase acetate assimilation pathway nor the TCA cycle enzymes (citrate synthase and aconitase) exclude fluorinated substrates based on *in vitro* biochemical characterization. Furthermore, disruption of the fluoroacetate resistance gene encoding a fluoroacetyl–CoA thioesterase (FlK) does not appear to lead to an observable growth defect related to organofluorine production. By showing that a switch in central metabolism can mediate and control molecular fluorine incorporation, our findings reveal a new potential strategy toward diversifying simple fluorinated building blocks into more complex products.

Graphical abstract

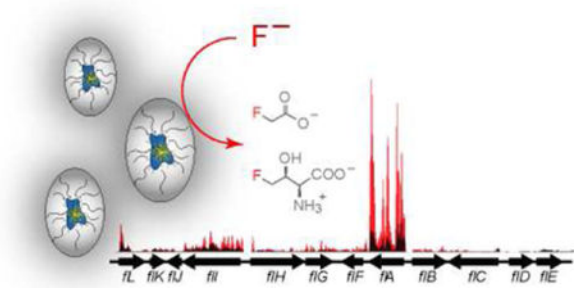

[*]**Corresponding Author**: mcchang@berkeley.edu.

Supporting Information. Full description of materials and methods, sequences of oligonucleotides, genome assembly statistics, gene cluster diagrams, RNAseq and DNA microarray data, SDS–PAGE, phylogenetic and biochemical data for enzymes, and data for knockout strains. This material is available free of charge via the internet at http://pubs.acs.org.

The continuing search for new biodiversity has yielded the discovery of many organisms with unusual chemical behaviors. One interesting chemical phenotype that has been observed in nature is the ability of *Streptomyces cattleya*, a soil–dwelling bacterium, to catalyze the formation of C–F bonds with fluoride as an environmentally green and abundant fluorine donor.(1, 2) Unlike other halogen–containing natural products (X = Cl, Br, I) that number in the thousands,(3) organofluorine compounds are quite rare(2, 4, 5) and relegated to a small number of compounds mostly derived from the fluoroacetate pathway (Scheme 1A).(6–8) This dearth of naturally–occurring compounds containing fluorine is especially striking given that fluorination has emerged as a particularly powerful tool for improving the efficacy of small–molecule drugs of synthetic origin for activity towards biological targets.(9–11) Even with the limited examples available, site–specific fluorination is also highly effective in a biological milieu as fluoroacetate is a simple yet highly toxic molecule that is capable of inactivating the tricarboxylic acid cycle with the substitution of a single hydrogen substituent for fluorine (Scheme 1B).(12, 13)

Our group is interested in exploring the fluorine physiology of *S. cattleya*, which is the only genetic host characterized to date that encodes a C–F bond forming enzyme,(14, 15) with the overall goal of elucidating how living systems handle this unique element in a cellular environment. Beyond fundamental studies directed at exploring how new and exotic chemical phenotypes evolve, we also hope to develop an understanding of cellular organofluorine management that could help to expand the synthetic biology of fluorine by engineering pathways for production of complex organofluorines from these simple building blocks. We therefore set out to study the metabolic machinery that underlies the fluorine physiology of *S. cattleya* using a combination of genomic, genetic, and *in vitro* biochemical methods. From these studies, we find that organofluorine biosynthesis is both fluoride– and growth phase–regulated, which provides a temporal mechanism to avoid endogenous fluoroacetate poisoning as it is only produced when cell growth and the TCA cycle shut down. This pattern of production is consistent with the behavior of other streptomycetes, where secondary metabolism is typically turned on during stationary phase(16) and supports the hypothesis that organofluorine production constitutes a normal cellular function for *S. cattleya* despite the apparent lack of gene clustering in the downstream steps of the fluoroacetate pathway. Indeed, the fluorinase, which catalyzes the C–F bond forming reaction, is the sixth most highly transcribed gene in the genome in the presence of fluoride, which is consistent with its slow rate of turnover(14) and further implies that fluorine secondary metabolism plays a major role in the *S. cattleya* life cycle.

RESULTS and DISCUSSION

Assembly of a *de novo* working genome sequence of *S. cattleya* using short reads

In order to gain insight into the organofluorine biosynthetic potential of *S. cattleya*, we decided to utilize next–generation sequencing methods to assemble a *de novo* draft genome sequence as a broad and non–biased approach to characterizing its genetic content (Figure S1). The reads were initially assembled using Velvet v. 1.0.14,(17) Image,(18) and CAP3(19) to produce a genome of 8.07 Mb over 154 contigs with an N_{50} of 133 kb (Table S2). For comparison, we also tested a newer and more automated short–read assembler,

SOAPdenovo63mer v 1.05,(20) to produce an assembly of 8.00 Mb over 192 contigs with an N_{50} of 158 kb (Table S2).

The completed genome of *S. cattleya* has been recently reported and deposited with the NCBI(21) and can be used for comparison of the quality of both of the Illumina–based assemblies (Figure S2 and S3). NUCMER from the MUMMER package(22) was used to map the contigs from the assemblies to the complete genome. The draft genomes obtained from Velvet and SOAPdenovo mapped to the completed genome with overall error rates of 0.06% and 0.02%, respectively. In the Velvet assembly, 34% of the contigs in the draft genome mapped directly to the complete genome with an additional 33% of contigs containing small insertions or deletions (37 base average length). The remaining contigs (31%) align well at the local level with the reference genome, but contain an incorrect scaffolding event from the initial Velvet assembly (Figure S2) that joins distant parts of the chromosome within the same contig. In comparison, the majority of the SOAPdenovo assembly (95% of contigs) maps directly to the reference with no scaffolding errors and a small number of contigs (4%) with insertions or deletions of moderate size (305 base average length). Regions in the complete *S. cattleya* genome that were absent from either the Velvet (70 regions, 49 kb) or SOAPdenovo (136 regions, 101 kb) assemblies mainly resulted from gaps located in repetitive regions of the genome (rRNA, transposase and polyketide coding sequences; Table S3), demonstrating the known difficulty of assembling redundant sequences using very short reads.

Fluorometabolism is regulated both by fluoride and the *S. cattleya* life cycle

Overall, it appears as if *S. cattleya* contains more copies of the pathway enzymes compared to other sequenced streptomycetes, which could possibly serve as a rich source of enzymes with fluorine specificity (Table S4). We hypothesized that expression of genes specifically involved in fluorometabolism could be regulated by the presence of fluoride given its potentially low bioavailability. Indeed, numerous putative transcription factors are found within the fluorinase (*flA*) gene cluster although none appear to be homologous to a reported chloride–dependent transcription factor.(23) We consequently cultured *S. cattleya* in GYM media at pH 5 in order to facilitate fluoride uptake and tracked the uptake of fluoride, production of organofluorines over time, and collected biomass at different stages of metabolism (Figure 1AB). We initially screened and sequenced cDNA libraries prepared from cultures 0.5, 2, 6, and 44 h after fluoride addition (Figure S4) using the Illumina platform in order to find the onset of fluoride-based differential gene expression. The short reads were mapped with BWA(24) to both the complete NCBI genome sequence as well as our draft genome sequence to avoid any inconsistencies in ORF identification. We further validated the results from 48 h time point by sequencing independent 48 h cDNA libraries as well as by comparison to results obtained from a custom microarray designed from our draft genome sequence (Figure S5).

Based on read–mapping to the *flA* gene cluster, it is clear that the fluorinase is significantly more highly expressed in the presence of fluoride than other genes in the cluster (Figure 1D). Indeed, it appears to be the most highly expressed gene of known function (sixth overall) in the entire genome 48 h after fluoride addition (Figure 1C) and upregulated

approximately 2.8–fold in response to fluoride. The expression of *flA* is also subject to strong temporal control with up-regulation tied to the onset of stationary phase, which is often observed in genes involved in secondary metabolite bio-synthesis.(25) The gene encoding fluoroacetyl–CoA specific thioesterase, FlK, was found to be constitutively expressed at low level, which is consistent with its role in resistance against fluoroacetate poisoning. Examining putative members of the fluoroacetate/fluorothreonine pathway (Scheme 1A) indicated that the 5′–fluorodeoxyadenosine phosphorylase (FlB), the fluoroacetaldehyde dehydrogenase (FAlDH), and the fluorothreonine (FT) transaldolase shared the same transcriptional response pattern with late–stage upregulation based on fluoride addition (Figure 2AB). However, none of the paralogs of either the methylthioribose–1–phosphate isomerase (MRI) or the fuculose–1–phosphate (F1P) aldolase appear to be transcriptionally activated by fluoride or within the same timeframe (Figure 2C–E). Nevertheless, these genes are indeed expressed but may be constitutively active or regulated at a post–transcriptional level.(26)

Identification and characterization of an unusual MRI fusion enzyme (MRI2)

The most unusual characteristic exhibited by *S. cattleya* revealed by the genome sequence perhaps occurs in the third step of the proposed pathway involving the MRI (Scheme 1A). While it shares a copy of the MRI conserved in streptomycetes (*mri1*) (Figure S7), *S. cattleya* also contains a second unusual MRI (*mri2*) fused to a class II aldolase fold that demonstrates homology to methylthioribulose–1–phosphate (MTRu1P) dehydratases and F1P aldolases and could catalyze the downstream step in either methionine salvage or fluorometabolite biosynthesis, respectively. Although the methionine salvage pathway varies in its distribution across the sequenced streptomycetes, both *S. avermitilis* and *S. scabiei* contain genes encoding separate MRIs and MTRu1P dehydratases that lie on opposite strands. Indeed, the only homologs to the MRI/MTRu1P dehydratase fusion in the non–redundant protein database come from the actinomycete, *Nocardia farcinica*, one of which is clustered with genes involved in acyl–CoA metabolism (Figure S8). Interestingly, the MRI2 fusion enzyme in *S. cattleya* is directly adjacent to a secondary metabolite cluster encoding the production of a hybrid polyketide/nonribosomal peptide (Figures S9–S10), which could potentially implicate the use of an unknown fluorinated subunit as a vehicle for fluorine introduction into a complex natural product in a manner analogous to chlorine in salinosporamide A.(27)

The shared MRI (MRI1) had previously been shown to accommodate fluorine as a substituent in place of the thiomethyl group. We therefore set out to biochemically characterize the MRI fusion enzyme (MRI2). *In vitro* studies indicate that MRI2 can utilize fluorinated substrates and that the function of the C–terminal fusion is the MTRu1P dehydratase reaction utilized in methionine salvage (Figure S11). Interestingly, no MTRu1P intermediate was observed with the thiomethyl–substituted substrate, possibly implicating substrate channeling or local concentration effects resulting from the fusion of the two activities that could distinguish the two MRI-dependent pathways *in vivo*.

In order to further assess the role of MRI1 and MRI2 in fluoroacetate (**6**) and fluorothreonine (**7**) production, we disrupted the genes in the *S. cattleya* chromosome via a

stable double–crossover. *S. cattleya* Δ*mri1* continues to exhibit an organofluorine profile similar to wildtype *S. cattleya* (with accelerated fluoride uptake), while the Δ*mri2* strain appears to have lost the ability to produce unidentified and low–abundance organofluorines observed in the wildtype strain (Figures 3 and S12). Although the disappearance of the unidentified organofluorines in Δ*mri2* profile is interesting with regard to the production of novel fluorinated natural products, these results indicate that neither MRI1 nor MRI2 appear to be specifically dedicated to fluoroacetate (**6**) and fluorothreonine (**7**) biosynthesis. In contrast, the Δ*mri1*Δ*mri2* double–knockout strain biosynthesizes only low levels of unidentified organofluorines that are different than the wildtype, Δ*mri1*, and Δ*mri2* strains under the same growth conditions without producing fluoroacetate (**6**) or fluorothreonine (**7**) (Figure 3). These observations support the model that an MRI-catalyzed step is indeed on pathway to fluoroacetate and fluorothreonine production as previously proposed(28) and that disruption of either *mri1* or *mri2* can be compensated by the second copy. However, it is difficult to conclude whether the change in organofluorine profile is related to direct disruption of the biosynthetic pathway or by regulatory changes tied to the *S. cattleya* growth and metabolic cycle since the Δ*mri1*Δ*mri2* strain maintains a deficiency in fluoride uptake as well as growth difference in liquid and on solid media (in the presence and absence of fluoride) that may be related to those reported for gene disruption and overexpression in the *mri1* locus for related actinomycetes (Figure S12).(29, 30)

FlK is not absolutely required for fluoroacetate resistance

A major question that we set out to explore is how *S. cattleya* is able to manage the toxic intracellular production of fluoroacetate (**6**), given its high effectiveness as an inhibitor of the TCA cycle (Scheme 1B). The fluoroacetyl–CoA (**9**) specific thioesterase, FlK, has been proposed to be involved in resistance(31) as it can selectively reverse the formation of fluoroacetyl–CoA (**9**) with a 10^6–fold selectivity over acetyl–CoA (**10**) and has been shown to confer fluoroacetate (**6**) resistance to *E. coli* (Scheme 1B).(32) However, FlK may not be the sole source of fluoroacetate (**6**) resistance, which could also involve acetate (**8**) assimilation, fluorocitrate (**11**) production, or aconitase reactivity with fluorine–based enzyme selectivity. To test this possibility, we first disrupted the *flK* gene in the *S. cattleya* chromosome by homologous recombination and characterized the resulting Δ*flK* strain with respect to fluoroacetate (**6**) resistance. Although the *ΔflK* strain retains a slight growth defect, it does not demonstrate any appreciable change in organofluorine production, growth rate, or final optical density resulting from fluoride or fluoroacetate (**6**) addition under organofluorine production conditions (Figure S13). Thus, any FlK–independent resistance mechanisms identified in this study could provide a roadmap for constructing a fluoroacetate–resistant host that retains the ability to generate and work with the fluoroacetyl–CoA (**9**) building block for downstream production of complex organofluorines.

S. cattleya has a lowered capacity for acetate assimilation

Analysis of the *S. cattleya* genome shows that it contains a single copy of a malate synthase but is missing an isocitrate lyase that would be required to constitute a functional glyoxylate shunt, which is canonically utilized for cell growth on acetate (**8**). The absence of a complete

glyoxylate shunt may indicate that *S. cattleya* may be able to reduce fluoroacetate (**6**) entry into the TCA cycle and the resulting toxicity by avoiding utilization of acetate (**8**) for cell growth. Indeed, our initial studies show that *S. cattleya* does not grow on acetate (**8**) as a sole carbon source under conditions in which *S. coelicolor* can. Other pathways for acetate (**8**) uptake and activation to acetyl–CoA (**10**) include the acetate kinase (AckA)/phosphotransacetylase (PTA) and the acetyl–CoA synthetase (ACS) pathways (Scheme 1B). Similar to five streptomycetes with completely sequenced and annotated genomes (*S. coelicolor, S. avermitilis, S. scabiei, S. bingchenggensis* and *S. griseus*), *S. cattleya* contains one copy of each of these genes.

These enzymes were cloned from *S. cattleya* genomic DNA, heterologously expressed in *E. coli* (Figure S14). The steady–state kinetic parameters for fluorinated and nonfluorinated substrate congeners were then measured and compared to orthologous enzymes from *E. coli*, a bacterium known to be susceptible to fluoroacetate (**6**) poisoning via the AckA/PTA pathway.(33) Studies on the *S. cattleya* ACS suggest that *S. cattleya* is unable to assimilate fluoroacetate (**6**) through its ACS and are in agreement with those from the *E. coli* ACS, implying that fluoroacetate (**6**) is not imported through this pathway (Table 1). Examination of the kinetic parameters for AckA and PTA individually from *S. cattleya* and *E. coli* suggest *S. cattleya*'s enzymes are capable of assimilating acetate (**8**) and fluoroacetate (**6**) with a lower overall catalytic efficiency than those of *E. coli*, but with no additional selectivity with respect to fluorine (Table 1).

The *S. cattleya* TCA cycle enzymes do not exclude fluorinated substrates

The most transferable fluoroacetate (**6**) resistance mechanism would either be a citrate synthase (CS) that excludes fluoroacetyl–CoA (**9**) as a substrate or an aconitase that is resistant to fluorocitrate (**11**) poisoning because either enzyme could be used to replace a synthetic host's native enzymes and allow downstream fluoroacetyl–CoA (**9**) utilization without toxicity. *S. cattleya* contains four predicted CS paralogs (Cit1–4), with Cit1 as the primary CS (Figure S15) and Cit2 as the next most highly transcribed CS. We cloned and expressed Cit1, Cit2, CitA, and GltA from *S. cattleya*, *S. coelicolor*, and *E. coli* (Figure S16) and determined their kinetic parameters with respect to acetyl–CoA (**10**) and fluoroacetyl–CoA (**9**) as well as oxaloacetate for the *S. cattleya* citrate synthases (Table 2, Figure S17). Despite its high sequence identity to CitA,(34) Cit1 exhibits lower overall catalytic activity and it lacks positive cooperativity based on its Hill coefficient. Multiple sequence alignment of Cit1 with ten orthologs and GltA show that Cit1 contains several mutations of highly conserved residues at the predicted regulatory interfaces(35) despite its very high overall similarity (Figure S18). Therefore, Cit1 may still have specialized properties with regard to regulation despite its similarity to CitA and GltA under *in vitro* assay conditions. In comparison, a secondary CS from *S. cattleya*, Cit2, displays a k_{cat}/K_M that is an order of magnitude higher compared to the other characterized CSs but is not highly transcribed under these conditions. Further downstream, it appears as if the sole *S. cattleya* aconitase is susceptible to fluorocitrate (**11**) inhibition based on assays of cell lysates prepared from cultures grown both in the presence and absence of fluoride to control for possible fluoride activation of an auxiliary resistance gene (Figure S20). Taken together, it seems as if the *S.*

cattleya TCA cycle enzymes remain competent for the lethal synthesis of fluorocitrate (**11**) and the resulting shutdown of the aconitase–catalyzed step.

Temporal control of fluoroacetate toxicity and fluoride–dependent transcriptional changes in the TCA cycle

Since our biochemical studies point to the conclusion that mechanisms based on enzymatic fluorine selectivity do not seem to be the major contributor to *S. cattleya* organofluorine resistance, we then sought to examine changes at the transcriptional level that could also provide resistance by temporal coordination between fluorometabolism and central metabolism. In comparing the expression level of TCA cycle genes over time and with addition of fluoride, it appears as if they are highly responsive to growth phase but not to fluoride (Figures 4 and S21). Thus it appears as if organofluorine biosynthesis is controlled by the cell cycle rather than the converse. Interestingly, an apparent operon of α–ketoglutarate dehydrogenase genes was upregulated in response to fluoride, which may imply that carbon enters the TCA cycle through glutamate or glutamine in order to bypass the CS– and aconitase–dependent steps (Figures 4 and S21). Thus, *S. cattleya* likely only turns on the fluorometabolite gene cluster and other related genes once the TCA cycle flux decreases as cells exit exponential growth and biomass accumulation. However, the fluoride dependence of *flA* expression indicates that there are several layers to the regulatory network involving fluoroacetate (**6**) and fluorothreonine (**7**) production.

Overall transcriptional response to fluoride

Other transcriptional responses to the presence of fluoride are notable 48 h after the addition of fluoride. In particular there appears to be a change in 5– and 3–carbon metabolism, which are substrates and products of the fluoroacetate pathway, respectively. A copy of the glyceraldehyde–3–phosphate dehydrogenase, distinct from the glycolytic copy, is the third most highly upregulated protein (27–fold) in the presence of fluoride. Additionally, glycerol–3–phosphate dehydrogenase and glycerol kinase are also upregulated (5–fold each). Changes in 5–carbon metabolism are also observed with upregulation of xylose isomerase (2.9–fold) and xylulose kinase (2.6–fold) and down regulation of L–ribulose–5-phosphate–4–epimerase (2.5–fold), L–ribulokinase (2.5–fold), and L–arabinose isomerase (2.4–fold) in the presence of fluoride. These changes in transcription may be involved with organofluorine biosynthesis as 5–carbon sugar related transcriptional responses could be an alternative approach controlling pools of the C_5 organofluorine intermediates in the cell.

BiNGO(36) was used to examine functional enrichment of differentially expressed genes in the presence of fluoride based on clusters of orthologous groups (COG) categories provided by the IMG–ER annotation (Figure 5). The energy production and conversion COG appears to be overrepresented in genes upregulated in the presence of fluoride, with the majority of these enzymes predicted to be involved in redox reactions (dehydrogenases, reductases and oxidases). Another enriched COG is amino acid transport and metabolism, among which are aminotransferases, proteases, and amino acid transporters. The final significantly upregulated COG is secondary metabolite biosynthesis, transport, and catabolism, consisting mostly of polyketide synthases and their accessory proteins. For downregulated categories, the signal transduction and inorganic ion transport and metabolism COGs are over

represented, with the latter resulting from genes predicted to be involved in iron transport and siderophore related processes.

Conclusions

Our group is interested in understanding the underlying design principles that allow an organism to manage an unusual element like fluorine with the long–term goal of developing a template for expanding the scope of enzymatic fluorination chemistry in living systems. Towards this effort, we have used a combination of genomic, cell profiling, genetic, and biochemical approaches to explore and elucidate the systems–level behavior of *S. cattleya* with respect to fluorine and organofluorine resistance. In this regard, organofluorine biosynthesis appears to be transcriptionally regulated both by fluoride as well as by growth phase. Both the genes encoding the putative FAlDH and the FT transaldolase share this behavior, which is consistent with a biosynthetic role in fluoroacetate (**6**) and fluorothreonine (**7**) production, whereas none of the MRI or F1P aldolase paralogs follow the same transcriptional pattern.

Using biochemical methods to assess the fluorine specificity of the acetate activation systems (AckA/Pta and ACS), CS, and aconitase, we have shown that the enzymes from *S. cattleya* do not appear to exclude the fluorinated metabolites as the major mechanism of resistance. Instead, the management of organofluorine toxicity appears to be highly controlled at the transcriptional level where organofluorine production is initiated in stationary phase only after the TCA cycle is shut down. In contrast to organofluorine biosynthesis, we observe no fluoride dependence to the transcription of TCA cycle enzymes, implying that organofluorine production does not control the growth phase of *S. cattleya*. However, the primary CS, Cit1, does appear to have different biochemical and regulatory properties compared to closely related orthologs that may lead to differences in TCA cycle behavior at the post–translational level. Other global shifts in metabolic flux could result from re–routing of carbon flux through glutamate–based anaplerotic reactions based on the upregulation of a secondary α–ketoglutarate dehydrogenase operon as well as changes in 3– and 5– carbon metabolism. These results suggest a metabolic framework to begin exploring the engineered biosynthesis of complex organofluorines from fluoroacetate while avoiding cellular toxicity from the fluorinated building block.

While growth phase-controlled production of secondary metabolites in streptomycetes by either global or pathway-specific transcription factors(25) is common, the additional layer of response to fluoride could be interesting with regard to identifying new mechanisms of fluoride–based gene regulation. As there are no fluoride–dependent protein transcription factors known at this time, it is also possible that a constitutively–produced organofluorine could be responsible for amplifying expression of pathway genes. There are several predicted transcription factors found within the *flA* gene cluster, including one (*flG*) that is upregulated 2.7–fold in the presence of fluoride. However, analysis of the upstream regions of fluoride–regulated pathway genes did not yield any clear consensus sequence, indicating that their transcription may not be controlled by a single specific regulator. Indeed, several predicted transcriptional regulators are differentially expressed in the presence of fluoride, including a member of the *whiB* family thought to be involved in cellular differentiation,(37)

which interestingly appears not to be conserved in other sequenced streptomycetes. Another possibility is that fluoride–sensing mechanisms based on structural RNAs could be used to control the expression level of a key regulator. In this regard, *S. cattleya* appears to contain a member of recently reported *crcB* family of fluoride riboswitches(26) (Figures S22–23). However, the known consensus sequences are not found within the *flA* gene cluster and may suggest a different mechanism or RNA sequence motif.

In addition to elucidating how organofluorine synthesis may be controlled *in vivo*, we are also interested in exploring the question of whether complex organofluorines already exist in *S. cattleya*. Although neither MRI1 nor the MRI2 fusion enzyme appears to be dedicated to fluoroacetate (**6**) or fluorothreonine (**7**) biosynthesis, the disruption of both genes leads to the loss of organofluorine production, which may result either from direct involvement of both enzymes in organofluorine production or loss of growth phase activation of fluorometabolite biosynthesis. The disappearance of low abundance organofluorines from the wildtype *S. cattleya* profile upon disruption of *mri2* is also interesting with regard to the production of uncharacterized fluorinated natural products. Biochemical characterization of the MRI1 fusion enzyme indicates that it is competent to react with fluorinated substrates to produce 2,3–diketo–5–fluoropentyl–1–phosphate, which could be on pathway to generate a fluorinated amino acid via the methionine salvage pathway. Like other actinomycetes, *S. cattleya* demonstrates a high potential for production of secondary metabolites from acetate– and amino acid–derived building blocks, some of which may possibly accept alternative building blocks (Table S5–6) and is an interesting area for further exploration.

METHODS

De novo assembly and annotation of the *S. cattleya* NRRL 8057 genome from short reads

S. cattleya ATCC 35852 genomic DNA was isolated using a modified salting–out protocol(38) and assayed for purity by amplification and sequencing of the 16s rRNA genes. Four paired–end libraries (Figure S1) were sequenced on an Illumina Genome Analyzer to generate 45 base forward and reverse reads (1.5 Gb) and 61 base forward and 45 base reverse reads (2.7 Gb). The short reads were assembled using Velvet v. 1.0.14(17) and Image(18) or SOAP v. 1.05 and Gapcloser.(20) Putative open reading frames as well as structural RNAs were detected and annotated by submission to the IMG Expert Review pipeline at the Joint Genome Institute.(39)

Preparation of mRNA for characterization of the *S. cattleya* fluoride–dependent transcriptional response

S. cattleya was grown in GYM media (pH 5.0) with glass beads (5 mm) to disperse growth. Sodium fluoride (2 mM) was added to the appropriate cultures 24 h after inoculation. Biomass was collected 0.5, 2, 6, 24, and 48 h after the addition of fluoride. Total RNA was isolated using Qiagen RNeasy Mini Kit and rRNA was depleted in two rounds using the MICROBExpress Kit (Ambion).

RNA sequencing

mRNA was fragmented before synthesizing cDNA for library preparation. Each lane of RNAseq reads was mapped to the completed genome of *S. cattleya*(21) using BWA.(24) Reads per feature were then extracted from the alignment file using HTseq–count.(40) The counts per feature for each condition and time point were quantile normalized using the preprocessCore R package.(41) For differential expression analysis, Multiexperiment Viewer (MeV) was used to perform statistical analysis using edgeR.(42)

DNA microarrays

Custom DNA microarrays (Agilent Technologies) were designed using eArray for a total of 15,744 60–mer probes. One sample t–test was applied to log2 fold changes to determine differentially expressed genes.

Construction of vectors for protein expression and isolation of His–tagged proteins

Expression plasmids were constructed by amplification of target genes (Table S1) from the appropriate genomic DNA and insertion into the pET16 or 1b (Addgene 29653) vectors. His–tagged proteins were expressed in *E. coli* BL21(de3) at 16°C and isolated using standard methods. pRARE2 was co–transformed for the expression of *Streptomyces* spp. and *Bacillus subtilis* proteins.

Enzyme assays

Acetyl–CoA synthetase,(43) acetate kinase,(43) phosphotransacetylase,(44) and citrate synthase(44) were assayed using literature methods. Phosphotransacetylase activity was also determined in the acyl–CoA forming direction using a discontinuous HPLC assay. MRI2 was assayed using methylthioribose–1–phosphate prepared according a modified literature protocol(45) and monitored by LCMS.

Measurement of aconitase assay in *S. cattleya* cell lysates

S. cattleya cell lysates were prepared from cultures using lysozyme (1 mg mL^{-1}) treatment followed by passage through a French pressure cell (25,000 psi). Aconitase was recharged with iron and assayed using a modified literature method to monitor the production of isocitrate.(46)

Construction of S. cattleya Δmri1::Hm^R, Δmri2::Am^R, Δmri1::Hm^R Δmri2::Am^R, and ΔflK::Am^R strains

Plasmids for gene disruption contained a cassette consisting of an apramycin (Am) or hygromycin (Hm) resistance marker and an origin of transfer (*oriT*) flanked by *S. cattleya* genomic DNA sequence derived from the upstream and downstream regions (2 kb) of the open reading frame to be disrupted. Plasmids were transferred into *S. cattleya* by conjugation with *E. coli* GM272 pUZ8002 using a modified literature protocol.(38) Disruption of the target gene was verified by sequencing following isolation of the exconjugants.

Organofluorine production

Single colonies of *S. cattleya* wildtype, Δ*mri1::Hm*^{R}, Δ*mri2::Am*^{R}, and Δ*mri1::Hm*^{R} Δ*mri2::Am*^{R} strains were grown in GYM pH 5 with glass beads. After 24 h, sodium fluoride (2 mM) was added to the cultures and aliquots were removed at 1, 2, 3, 6, 9, 12, and 15 d after fluoride addition. Fluoride concentration in the culture supernatant was measured using a fluoride ion selective electrode (Mettler Toledo) and organofluorine production was monitored by ^{19}F NMR after lyophilizing the supernatant with a fluorouracil internal standard.

Complete Materials and Methods

Detailed procedures can be found in the Supporting Information.

Supplementary Material

Refer to Web version on PubMed Central for supplementary material.

Acknowledgments

We thank B. Thuronyi for cloning the *E. coli ackA* and *pta* genes and J. Gomez–Escribano and M. Bibb (John Innes Centre) for materials and assistance in developing conjugation protocols for *S. cattleya*. We would also like to acknowledge B. Curry (Agilent Technologies) and C. Canlas (College of Chemistry NMR Facility) for assistance in analysis of custom microarrays and ^{19}F NMR, respectively.

Funding Sources

This work was funded by the generous support of the Arnold and Mabel Beckman Foundation, the Hellman Family Fund, and a National Institutes of Health New Innovator Award (1 DP2 OD008696). M.C.W. and A.M.W. also acknowledge the support of a National Institutes of Health NRSA Training Grant (1 T32 GMO66698) and a National Science Foundation Graduate Research Fellowship (to A.M.W.). The College of Chemistry NMR Facility at the University of California, Berkeley is supported in part by the National Institutes of Health (1S10RR023679-01 and S10 RR16634-01).

References

1. O'Hagan D. Recent developments on the fluorinase from *Streptomyces cattleya*. J Fluor Chem. 2006; 127:1479–1483.
2. Sanada M, Miyano T, Iwadare S, Williamson J, Arison B, Smith J, Douglas A, Liesch J, Inamine E. Biosynthesis of fluorothreonine and fluoroacetic acid by the thienamycin producer, *Streptomyces cattleya*. J Antibiot. 1986; 39:259–265. [PubMed: 3082840]
3. Gribble GW. The diversity of naturally produced organohalogens. Chemosphere. 2003; 52:289–297. [PubMed: 12738253]
4. Gribble, GW. The Handbook of Environmental Chemistry. Springer-Verlag; Berlin: 2002. p. 121-136.
5. Fukuda K, Tamura T, Segawa Y, Mutaguchi Y, Inagaki K. Enhanced production of the fluorinated nucleoside antibiotic nucleocidin by a rifR-resistant mutant of Streptomyces calvus IFO13200. Actinomycetologica. 2009; 23:51–55.
6. Moss SJ, Murphy CD, O'Hagan D, Schaffrath C, Hamilton JTG, McRoberts WC, Harper DB. Fluoroacetaldehyde: A precursor of both fluoroacetate and 4-fluorothreonine in *Streptomyces cattleya*. Chem Commun. 2000:2281–2282.
7. Murphy CD, Moss SJ, O'Hagan D. Isolation of an aldehyde dehydrogenase involved in the oxidation of fluoroacetaldehyde to fluoroacetate in *Streptomyces cattleya*. Appl Environ Microbiol. 2001; 67:4919–4921. [PubMed: 11571203]

8. Deng H, Cross SM, McGlinchey RP, Hamilton JTG, O'Hagan D. In vitro reconstituted biotransformation of 4-fluorothreonine from fluoride ion: Application of the fluorinase. Chem Biol. 2008; 15:1268–1276. [PubMed: 19101471]
9. Smart BE. Fluorine substituent effects (on bioactivity). J Fluorine Chem. 2001; 109:3–11.
10. Biffinger JC, Kim HW, DiMagno SG. The polar hydrophobicity of fluorinated compounds. Chembiochem. 2004; 5:622–627. [PubMed: 15122633]
11. Müller K, Faeh C, Diederich F. Fluorine in pharmaceuticals: Looking beyond intuition. Science. 2007; 317:1881–1886. [PubMed: 17901324]
12. Clarke DD. Fluoroacetate and fluorocitrate: Mechanism of action. Neurochem Res. 1991; 16:1055–1058. [PubMed: 1784332]
13. Lauble H, Kennedy MC, Emptage MH, Beinert H, Stout CD. The reaction of fluorocitrate with aconitase and the crystal structure of the enzyme-inhibitor complex. Proc Natl Acad Sci. 1996; 93:13699–13703. [PubMed: 8942997]
14. Schaffrath C, Deng H, O'Hagan D. Isolation and characterization of 5′-fluorodeoxyadenosine synthase, a fluorination enzyme from *Streptomyces cattleya*. FEBS Lett. 2003; 547:111–114. [PubMed: 12860396]
15. Dong C, Huang F, Deng H, Schaffrath C, Spencer JB, O'Hagan D, Naismith JH. Crystal structure and mechanism of a bacterial fluorinating enzyme. Nature. 2004; 427:561–565. [PubMed: 14765200]
16. Bibb M. The regulation of antibiotic production in *Streptomyces coelicolor* A3(2). Microbiology. 1996; 142:1335–1344. [PubMed: 8704973]
17. Zerbino DR, Birney E. Velvet: Algorithms for de novo short read assembly using de Bruijn graphs. Genome Res. 2008; 18:821–829. [PubMed: 18349386]
18. Tsai I, Otto T, Berriman M. Improving draft assemblies by iterative mapping and assembly of short reads to eliminate gaps. Genome Biol. 2010; 11:R41. [PubMed: 20388197]
19. Huang X, Madan A. CAP3: A DNA sequence assembly program. Genome Res. 1999; 9:868–877. [PubMed: 10508846]
20. Li R, Li Y, Kristiansen K, Wang J. SOAP: Short Oligonucleotide Alignment Program. Bioinformatics. 2008; 24:713–714. [PubMed: 18227114]
21. Barbe V, Bouzon M, Mangenot S, Badet B, Poulain J, Segurens B, Vallenet D, Marlière P, Weissenbach J. Complete genome sequence of Streptomyces cattleya NRRL 8057, a producer of antibiotics and fluorometabolites. J Bacteriol. 2011; 193:5055–5056. [PubMed: 21868806]
22. Kurtz S, Phillippy A, Delcher A, Smoot M, Shumway M, Antonescu C, Salzberg S. Versatile and open software for comparing large genomes. Genome Biol. 2004; 5:R12. [PubMed: 14759262]
23. Sanders JW, Venema G, Kok J, Leenhouts K. Identification of a sodium chloride-regulated promoter in *Lactococcus lactis* by single-copy chromosomal fusion with a reporter gene. Mol Gen Genet. 1998; 257:681–685. [PubMed: 9604892]
24. Li H, Durbin R. Fast and accurate short read alignment with Burrows-Wheeler transform. Bioinformatics. 2009; 25:1754–1760. [PubMed: 19451168]
25. Bibb MJ. Regulation of secondary metabolism in streptomycetes. Current Opinion in Microbiology. 2005; 8:208–215. [PubMed: 15802254]
26. Baker JL, Sudarsan N, Weinberg Z, Roth A, Stockbridge RB, Breaker RR. Widespread genetic switches and toxicity resistance proteins for fluoride. Science. 2012; 335:233–235. [PubMed: 22194412]
27. Eustaquio AS, Pojer F, Noel JP, Moore BS. Discovery and characterization of a marine bacterial SAM-dependent chlorinase. Nat Chem Biol. 2008; 4:69–74. [PubMed: 18059261]
28. Schaffrath C, Cobb SL, O'Hagan D. Cell-free biosynthesis of fluoroacetate and 4-fluorothreonine in *Streptomyces cattleya*. Angew Chem Int Ed. 2002; 41:3913–3915.
29. Moker N, Brocker M, Schaffer S, Kramer R, Morbach S, Bott M. Deletion of the genes encoding the MtrA-MtrB two-component system of *Corynebacterium glutamicum* has a strong influence on cell morphology, antibiotics susceptibility and expression of genes involved in osmoprotection. Mol Microbiol. 2004; 54:420–438. [PubMed: 15469514]

30. Zahrt TC, Deretic V. An essential two-component signal transduction system in *Mycobacterium tuberculosis*. J Bacteriol. 2000; 182:3832–3838. [PubMed: 10851001]
31. Huang F, Haydock SF, Spiteller D, Mironenko T, Li TL, O'Hagan D, Leadlay PF, Spencer JB. The gene cluster for fluorometabolite biosynthesis in *Streptomyces cattleya*: A thioesterase confers resistance to fluoroacetyl-coenzyme A. Chem Biol. 2006; 13:475–484. [PubMed: 16720268]
32. Weeks AM, Coyle SM, Jinek M, Doudna JA, Chang MCY. Structural and biochemical studies of a fluoroacetyl-CoA-specific thioesterase reveal a molecular basis for fluorine selectivity. Biochemistry. 2010; 49:9269–9279. [PubMed: 20836570]
33. Brown TDK, Jones-Mortimer MC, Kornberg HL. The enzymic interconversion of acetate and acetyl-coenzyme A in *Escherichia coli*. J Gen Microbiol. 1977; 102:327–336. [PubMed: 21941]
34. Viollier PH, Minas W, Dale GE, Folcher M, Thompson CJ. Role of acid metabolism in *Streptomyces coelicolor* morphological differentiation and antibiotic biosynthesis. J Bacteriol. 2001; 183:3184–3192. [PubMed: 11325948]
35. Nguyen NT, Maurus R, Stokell DJ, Ayed A, Duckworth HW, Brayer GD. Comparative analysis of folding and substrate binding sites between regulated hexameric type II citrate synthases and unregulated dimeric type I enzymes. Biochemistry. 2001; 40:13177–13187. [PubMed: 11683626]
36. Maere S, Heymans K, Kuiper M. BiNGO: A Cytoscape plugin to assess overrepresentation of Gene Ontology categories in biological networks. Bioinformatics. 2005; 21:3448–3449. [PubMed: 15972284]
37. Chater KF. Regulation of sporulation in *Streptomyces coelicolor* A3(2): A checkpoint multiplex? Curr Opin Microbiol. 2001; 4:667–673. [PubMed: 11731318]
38. Kieser, T., Bibb, MJ., Buttner, MJ., Chater, KF., DA, H. Practical Streptomyces genetics. The John Innes Foundation; Norwich, England: 2000.
39. Markowitz VM, Mavromatis K, Ivanova NN, Chen IMA, Chu K, Kyrpides NC. IMG ER: A system for microbial genome annotation expert review and curation. Bioinformatics. 2009; 25:2271–2278. [PubMed: 19561336]
40. Anders S, Huber W. Differential expression analysis for sequence count data. Genome Biol. 2010; 11:1–12.
41. Bolstad BM, Irizarry RA, Åstrand M, Speed TP. A comparison of normalization methods for high density oligonucleotide array data based on variance and bias. Bioinformatics. 2003; 19:185–193. [PubMed: 12538238]
42. Saeed A, Sharov V, White J, Li J, Liang W, Bhagabati N, Braisted J, Klapa M, Currier T, Thiagarajan M, Sturn A, Snuffin M, Rezantsev A, Popov D, Ryltsov A, Kostukovich E, Borisovsky I, Liu Z, Vinsavich A, Trush V, Quackenbush J. TM4: A free, open-source system for microarray data management and analysis. BioTechniques. 2003; 34:374–378. [PubMed: 12613259]
43. Williamson JR, Corkey BE. Assays of intermediates of the citric acid cycle and related compounds by fluorometric enzyme methods. Method Enzymol. 1969:434–513.
44. Srere PA, Brazil H, Gonen L. The citrate condensing enzyme of pigeon breast muscle and moth flight muscle. Acta Chem Scand. 1963; 19:129–134.
45. Ashida H, Saito Y, Kojima C, Kobayashi K, Ogasawara N, Yokota A. A functional link between RuBisCO-like protein of Bacillus and photosynthetic RuBisCO. Science. 2003; 302:286–290. [PubMed: 14551435]
46. Henson CP, Cleland WW. Purification and kinetic studies of beef liver cytoplasmic aconitase. J Biol Chem. 1967; 242:3833–3838. [PubMed: 6037548]

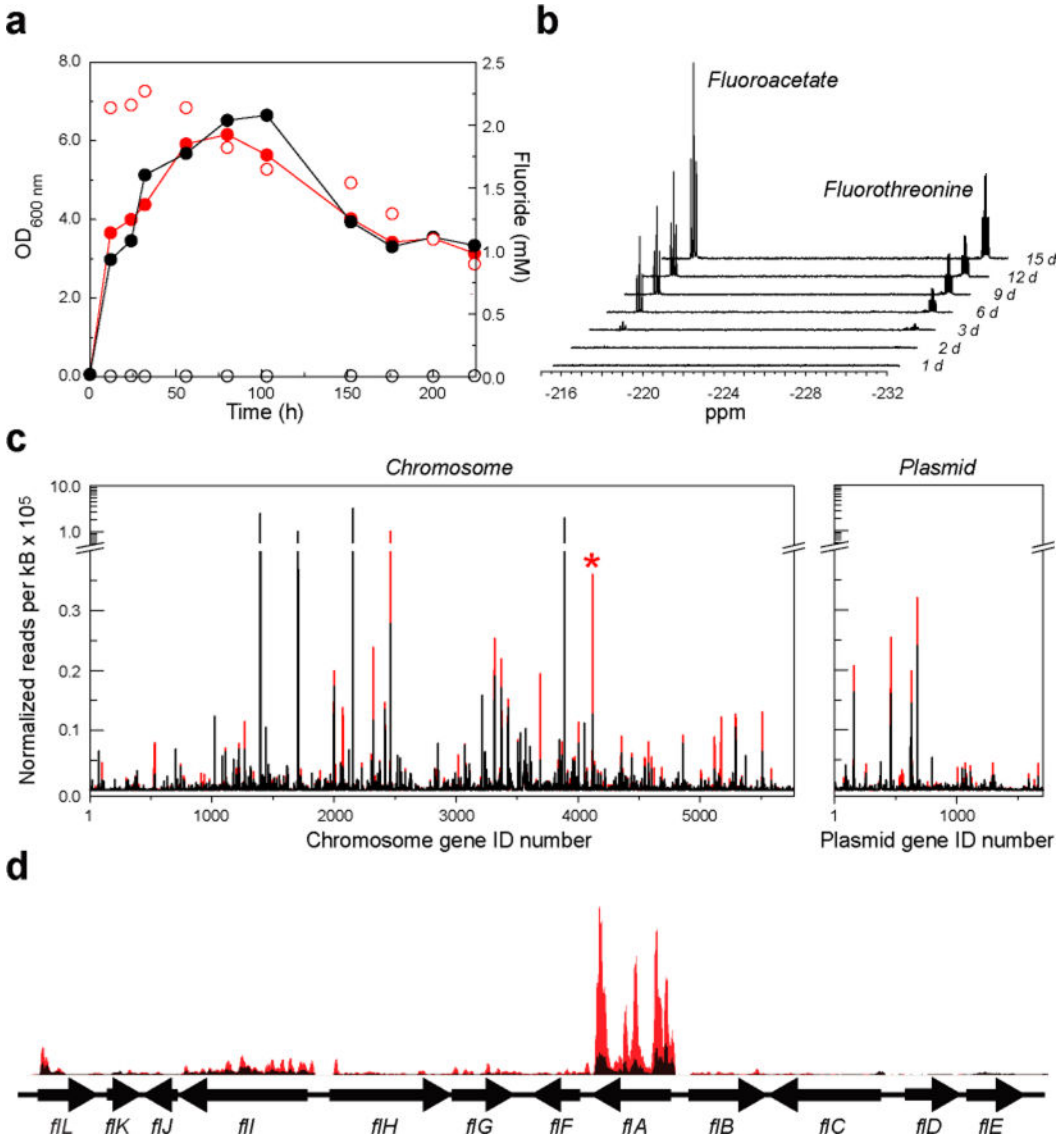

Figure 1.

Analysis of the fluoride response in *S. cattleya*. (a) Growth and fluoride uptake in *S. cattleya* cultures in GYM media at pH 5. Growth of cultures measured by $OD_{600\ nm}$ (filled circles) and fluoride concentration (open circles) with (red) and without (black) 2 mM sodium fluoride added 24 h after inoculation. (b) Monitoring organofluorine production by ^{19}F NMR in the culture supernatant. (c) Transcriptional landscape of *S. cattleya* 48 h after the addition (red) or no addition (black) of fluoride. Values are quantile normalized reads per kb for predicted protein coding sequences. The fluorinase (*flA*) is indicated by a star. (d) RNA sequencing reads mapped onto the fluorinase gene cluster 48 h after the addition of fluoride (red) compared samples with no added fluoride (black).

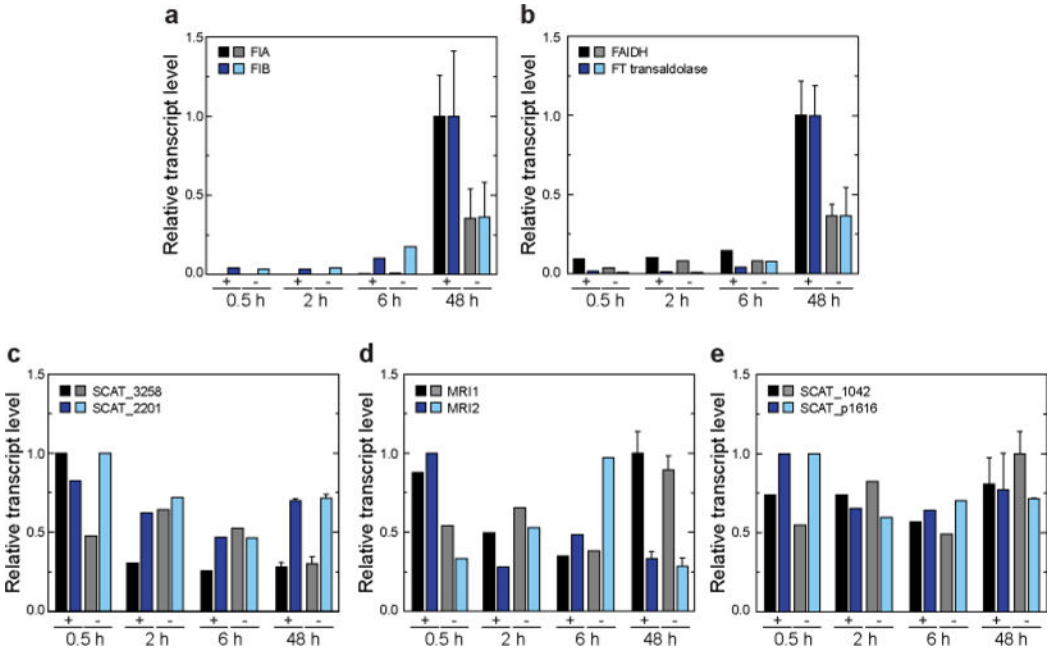

Figure 2.

Time– and fluoride–dependent changes in transcript levels of predicted pathway genes and their paralogs. Transcript levels were quantified by RNA sequencing 0.5, 2, 6, and 48 h after the addition of 2 mM sodium fluoride and compared to no addition. Values at 48 h are the mean of two replicates and error bars indicate one standard deviation. Transcription levels of reads per kb were normalized to the maximum value for each predicted open reading frame in parentheses. (a) FlA (36,036 reads/kb) and FlB (1,091 reads/kb) (b) the predicted fluoroacetaldehyde dehydrogenase gene (FAldH, 2,677 reads/kb) and the fluorothreonine transaldolase gene (FT transaldolase, 975 reads/kb), (c) methylthioadenosine phosphorylase paralogs (SCAT_3258, 432 reads/kb; SCAT_2201, 411 reads/kb), (d) MRI1 (192 reads/kb) and MRI2 (278 reads/kb), and (e) F1P aldolase paralogs (SCAT_1042, 241 reads/kb; SCAT_p1616, 78 reads/kb).

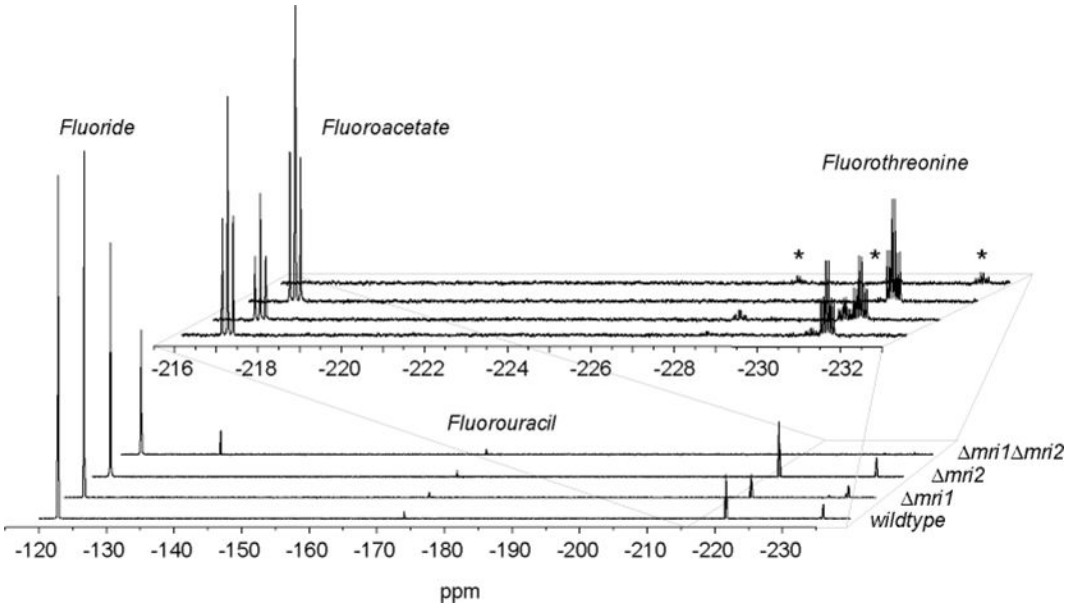

Figure 3.

Organofluorine production in *S. cattleya* and MRI knockout strains. ^{19}F NMR analysis of culture supernatants from wildtype, *Δmri1, Δmri2*, and *Δmri1Δmri2* strains of *S. cattleya* 6 d after the addition of sodium fluoride (2 mM).

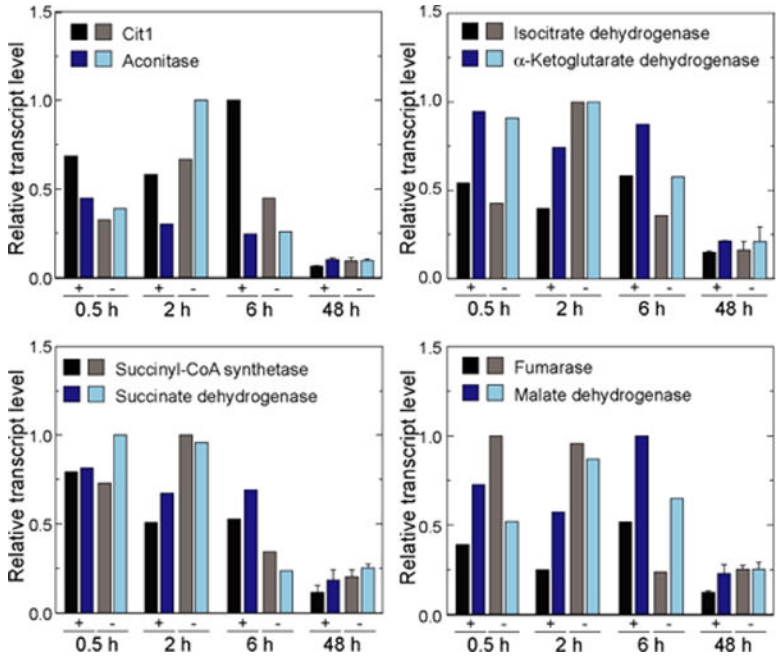

Figure 4.

Transcription patterns for TCA cycle genes with respect to fluoride and time. Transcript levels were quantified by RNA sequencing 0.5, 2, 6, and 48 h after the addition of 2 mM sodium fluoride and compared to no addition. Values at 48 h are the mean of two replicates and error bars indicate one standard deviation. Transcription levels of reads per kb were normalized to the maximum value for each predicted open reading frame in parentheses with a representative subunit given for multi–subunit enzymes. Time courses are shown for Cit1 (7,130 reads/kb), aconitase (4,238 reads/kb), isocitrate dehydrogenase (3,495 reads/kb), α–ketoglutarate dehydrogenase (3,094 reads/kb), succinyl–CoA synthetase (5,383 reads/kb), succinate dehydrogenase (2,050 reads/kb), fumarase (2,141 reads/kb), and malate dehydrogenase (6,207 reads/kb).

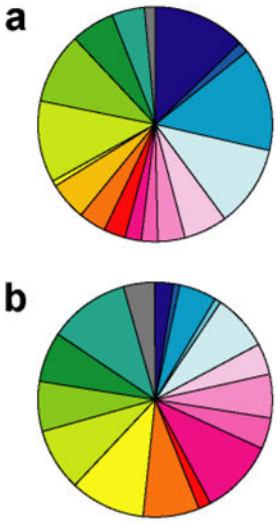

c

	Genome	Up	Down
Chromatin structure and dynamics	1 (0.03)	0 (0.00)	0 (0.00)
Energy production and conversion	248 (7.43)	17 (13.71)	3 (3.09)
Cell cycle control, cell division, chromosome partitioning	30 (0.90)	2 (1.61)	1 (1.03)
Amino acid transport and metabolism	299 (8.96)	19 (15.32)	6 (6.19)
Nucleotide transport and metabolism	71 (2.13)	0 (0.00)	1 (1.03)
Carbohydrate transport and metabolism	295 (8.84)	15 (12.10)	9 (9.28)
Coenzyme transport and metabolism	185 (5.54)	8 (6.45)	5 (5.15)
Lipid transport and metabolism	208 (6.23)	5 (4.03)	7 (7.22)
Translation, ribosomal structure/biogenesis	118 (3.54)	3 (2.42)	5 (5.15)
Transcription	497 (14.89)	3 (2.42)	12 (12.37)
Replication, recombination and repair	143 (4.28)	4 (3.23)	2 (2.06)
Cell wall/membrane/envelope biogenesis	165 (4.94)	5 (4.03)	9 (9.28)
Cell motility	4 (0.12)	0 (0.00)	0 (0.00)
Post-translational modification, protein turnover, chaperones	120 (3.59)	7 (5.65)	0 (0.00)
Inorganic ion transport and metabolism	121 (3.62)	1 (0.81)	12 (12.37)
Secondary metabolite biosynthesis, transport, catabolism	231 (6.92)	15 (12.10)	10 (10.31)
General function prediction only	515 (15.43)	13 (10.48)	8 (8.25)
Unknown function	250 (7.49)	8 (6.45)	8 (8.25)
Signal transduction mechanisms	246 (7.37)	6 (4.84)	13 (13.40)
Intracellular trafficking, secretion, vesicular transport	29 (0.87)	0 (0.00)	0 (0.00)
Defense mechanisms	72 (2.16)	2 (1.61)	5 (5.15)
Cytoskeleton	1 (0.03)	0 (0.00)	0 (0.00)
Total	**3338**	**124**	**97**

Figure 5.

COG categories for genes differentially expressed with respect to fluoride. COG categories were identified by the IMG–ER annotation pipeline. COG categories represented by genes that are (A) upregulated and (B) downregulated in the presence of fluoride at 48 h. (C) Comparison of COG category representation in the differentially expressed genes with that of the entire genome. The number of open reading frames represented by each COG are given and the percentage of total genes with COG categories are in parenthesis.

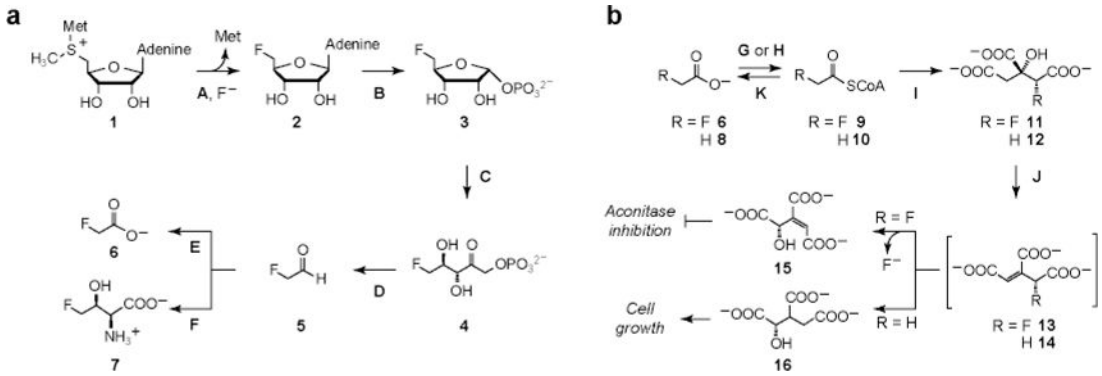

Scheme 1. Biological organofluorine pathways.[a]

[a](a) The proposed biosynthetic pathway for fluoroacetate and fluorothreonine in *S. cattleya*. *S*–adenosylmethionine (**1**), 5′–fluorodeoxyadenosine (**2**), 5–fluorodeoxyribose–1–phosphate (**3**), 5–fluorodeoxyribulose–1–phosphate (**4**), fluoroacetaldehyde (**5**), fluoroacetate (**6**), fluorothreonine (**7**). Fluorinase (FlA, **A**), 5′–fluorodeoxyadenosine or methylthioadenosine phosphorylase (FlB, **B**), methylthioribulose–1–phosphate isomerase (MRI, **C**), fucolose–1–phosphate aldolase (F1P aldolase, **D**), fluoroacetaldehyde dehydrogenase (FAldH, **E**), fluorothreonine transaldolase (FT transaldolase, **F**). (b) Lethal synthesis of fluorocitrate and inactivation of aconitase. Acetate (**8**), fluoroacetyl–CoA (**9**), acetyl–CoA (**10**), fluorocitrate (**11**), citrate (**12**), fluoroaconitate (**13**), aconitate (**14**), 4–hydroxy–transaconitate (**15**), isocitrate (**16**). Acetate kinase and phosphotransacetylase (AckA and Pta, **G**), acetyl–CoA synthase (ACS, **H**), citrate synthase (CS, **I**), aconitase (**J**), fluoroacetyl–CoA thioesterase (FlK, **K**).

Table 1

Kinetic parameters for acetate assimilation enzymes.[a]

			k_{cat} (s^{-1})	K_M (μM)	k_{cat}/K_M ($M^{-1}s^{-1}$)
ACS	*S. cattleya*	Acetate	40 ± 1	9 ± 1	(4.4 ± 0.5) × 10^6
		Fluoroacetate	2.03 ± 0.08	(5.2 ± 0.9) × 10^4	(3.9 ± 0.7) × 10^1
	E. coli	Acetate	1.04 ± 0.03	6 ± 1	(1.7 ± 0.3) × 10^5
		Fluoroacetate	0.14 ± 0.01	(8 ± 3) × 10^4	(1.8 ± 0.7) × 10^0
AckA	*S. cattleya*	Acetate	410 ± 20	(1.7 ± 0.2) × 10^4	(2.4 ± 0.3) × 10^4
		Fluoroacetate	1.04 ± 0.01	(5.7 ± 0.4) × 10^3	(1.8 ± 0.1) × 10^2
	E.coli	Acetate	(1.34 ± 0.03) × 10^3	(2.7 ± 0.2) × 10^4	(5.0 ± 0.4) × 10^4
		Fluoroacetate	6.7 ± 0.2	(3.3 ± 0.4) × 10^4	(2.0 ± 0.3) × 10^2
PTA	*S. cattleya*[b]	Acetyl-CoA	4.0 ± 0.2	200 ± 20	(2.0 ± 0.2) × 10^4
		Fluoroacetyl-CoA	160 ± 8	670 ± 70	(2.4 ± 0.3) × 10^5
	E. coli[c]	Acetyl-CoA	37 ± 1	160 ± 20	(2.3 ± 0.3) × 10^5
		Fluoroacetyl-CoA	430 ± 20	160 ± 30	(2.7 ± 0.5) × 10^6

[a] Initial rates for ACS and AckA were determined with respect to acetate (**8**) and fluoroacetate (**6**) while initial rates for PTA were determined with respect to acetyl–CoA (**10**) and fluoroacetyl–CoA (**9**). Kinetic parameters were obtained by nonlinear fitting of the dose–response curves to the Michaelis–Menten equation. All data are mean ± s.e. (n = 3).

[b] Rate in the acyl–CoA forming direction: acetyl–CoA 3.5 ± 0.1 μ M s^{-1} Δ M PTA^{-1}; fluoroacetyl–CoA 3.4 ± 0.1 μ M s^{-1} Δ M PTA^{-1}.

[c] Rate in the acyl–CoA forming direction: acetyl–CoA 32 ± 3 μ M s^{-1} μ M PTA^{-1}; fluoroacetyl–CoA 80 ± 10 μ M s^{-1} μ M PTA^{-1}.

Table 2

Kinetic parameters for selected citrate synthases.[a]

			k_{cat} (s^{-1})	$K_{0.5}$ (μM)	n	$k_{cat}/K_{0.5}$ (M^{-1} s^{-1})
S. cattleya	Cit1	Acetyl-CoA	8.0 ± 0.3	15 ± 2	1.0 ± 0.1	(5.3 ± 0.7) × 10^5
		Fluoroacetyl-CoA	3.3 ± 0.2	16 ± 4	0.8 ± 0.1	(2.2 ± 0.9) × 10^5
		Oxaloacetate	8.0 ± 0.6	130 ± 20	1.2 ± 0.1	(6 ± 1) × 10^4
	Cit2	Acetyl-CoA	34 ± 1	4.9 ± 0.4	1.7 ± 0.2	(6.9 ± 0.6) × 10^6
		Fluoroacetyl-CoA	1.12 ± 0.02	0.98 ± 0.05	2.0 ± 0.3	(1.14 ± 0.06) × 10^6
		Oxaloacetate	24.9 ± 0.6	3.8 ± 0.4	1.3 ± 0.2	(6.6 ± 0.7) × 10^6
S. coelicolor	CitA	Acetyl-CoA	17.9 ± 0.4	47 ± 2	1.9 ± 0.1	(3.8 ± 0.1) × 10^5
		Fluoroacetyl-CoA	1.94 ± 0.06	15.4 ± 0.8	1.7 ± 0.2	(1.26 ± 0.08) × 10^5
E. coli	GltA	Acetyl-CoA	80 ± 10	170 ± 60	0.8 ± 0.1	(5 ± 2) × 10^5
		Fluoroacetyl-CoA	1.22 ± 0.03	5.1 ± 0.3	1.9 ± 0.3	(2.4 ± 0.2) × 10^5

[a]Initial rates for all the citrate synthases were determined with respect to acetyl-CoA (**10**) and fluoroacetyl-CoA (**9**). Additionally, initial rates for the *S. cattleya* citrate synthases were determined with respect to oxaloacetate. Kinetic parameters were obtained by nonlinear fitting of the dose–response curve to the Hill equation. All data are mean ± s.e. (n = 3).